Published in final edited form as:
Hippocampus. 2010 April ; 20(4): . doi:10.1002/hipo.20648.

Dose-Dependent Long-Term Effects of Tat in the Rat Hippocampal Formation: A Design-Based Stereological Study

Sylvia Fitting[1,*], **Rosemarie M. Booze**[1,2], **Ulla Hasselrot**[1], and **Charles F. Mactutus**[1]

[1]Departments of Psychology, University of South Carolina, Columbia, South Carolina

[2]Department of Physiology, Pharmacology, and Neuroscience, University of South Carolina, Columbia, South Carolina

Abstract

The human immunodeficiency virus type 1 (HIV-1) protein transactivator of transcription (Tat) is believed to play a critical role in mediating central nervous system (CNS) pathology in pediatric HIV-1 infection. Long-term neurotoxicity was investigated in a design-based stereology study following intrahippocampal injection of Tat on postnatal day (P)10, a time period that approximates the peak in the rats' rate of brain growth and mimics clinical HIV-1 CNS infection at labor/delivery. The goal was to examine the impact of P10 intrahippocampal Tat injection on the anatomy of the adult hippocampus (5 month) to gain a better understanding about how timing of infection influences the rate of progression of pediatric HIV-1 infection [cf. Fitting et al. (2008a) Hippocampus 18:135–147]. Male P10 Sprague-Dawley rats were bilaterally injected with vehicle or one of three different doses of Tat (5, 25, or 50 μg). Unbiased stereological estimates were used to quantify total neuron number (Nissl stain) in five major subregions of the rat hippocampus: granular layer (GL), hilus of the dentate gyrus (DGH), cornu ammonis fields (CA)2/3, CA1, and subiculum (SUB). Glial cells (astrocytes and oligodendrocytes) were quantified in the DGH and SUB. No significant reduction of neuron number was noted for any of the five hippocampal subregions, in contrast to the very prominent reductions reported when Tat was administered on P1 [Fitting et al. (2008a) Hippocampus 18:135–147]. However, for glial cells, the number of astrocytes in the DGH and SUB as well as the number of oligodendrocytes in the DGH were linear dose dependently increased as a function of dose of Tat. In conjunction with previous stereological research [Fitting et al., (2008a) Hippocampus 18:135–147], the present data suggest that variability in the progression of pediatric HIV/acquired immunodeficiency syndrome (AIDS) may be better understood with the knowledge of the factor of timing of HIV-1 CNS infection.

Keywords

Tat; stereology; hippocampus; glia; neurons

INTRODUCTION

According to the latest global statistics, 400,000 children younger than 15 yr were newly infected with human immunodeficiency virus (HIV)/acquired immunodeficiency syndrome (AIDS) in 2007 (UNAIDS/WHO, 2007). Entry of the virus into the central nervous system

[*]Correspondence to: Sylvia Fitting, Department of Pharmacology and Toxicology, Virginia Commonwealth University, Richmond, VA 23298. sfitting@vcu.edu.

(CNS) occurs at an early stage of HIV type 1 (HIV-1) infection and contributes significantly to the development of neurological complications. The major source (>90%) of pediatric infection occurs through vertical transmission of the virus from the mother to the child [mother-to-child-transmission (MTCT)]. The actual timing of MTCT pre- and postnatally is not known but commonly accepted estimates suggest transmission occurs most frequently *in utero* between the 36th week of gestation and delivery (50%), 30% during labor, and 20% before the 36th week of pregnancy (Kourtis et al., 2001). In women who breastfeed, the number of MTCT cases occurring postnatally ranges from 15% (WHO, 2000) to 30–35% (Ogundele and Coulter, 2003). The latter estimate is reported for developing countries due to a complex mix of environmental, social, cultural, educational, and economical factors.

Treatment of pediatric HIV-1 infection with antiretroviral therapies has greatly improved the survival time and outcome of pediatric HIV-1-infection (Equils et al., 2000; Wolters and Brouwers, 2005). However, antiretroviral therapies and treatment of opportunistic infection do not eradicate the virus from the CNS. Longer survival times of children infected with HIV-1 as well as the mutation to more highly virulent and resistant forms of the virus have precipitated a recent increase in the development of neurological complications and psychological impairments (Gelbard and Epstein, 1995). Most commonly, HIV-1 infected children express delays in developmental milestones (Epstein et al., 1986), impairment in brain growth as well as progressive motor dysfunction (Mintz, 2005) and attentional and memory deficits (Fowler, 1994; Mintz, 1994). The progression of the CNS disease is reported to be quite variable in the pediatric HIV-1 population, ranging from rapid rates of progression and global neurodevelopmental deficits to much slower rates with mild impairments in selective domains of cognitive functioning (Blanche et al., 1990; Wiley, et al., 1990; Chearskul et al., 2002; Wolters and Brouwers, 2005).

The mechanisms of the HIV-1-mediated CNS disease are not completely understood. Some of the proposed mechanisms include macrophage and microglia invasion that results in neuronal injury and death (Gelbard et al., 1995; Krajewski et al., 1997), persistent infection of astrocytes (Tornatore et al., 1994), release of viral toxins (Jones et al., 2000; Valle et al., 2000; Annunziata, 2003), caspase-3 upregulation in apoptotic neurons (James et al., 1999), overexpression of chemokine receptors CCR5 and CXCR4 (Vallat et al., 1998), and alteration of the blood–brain-barrier (Annunziata, 2003). Because the virus does not infect neurons, it is suggested that the mechanism of HIV-1-induced neurotoxicity occurs indirectly (Takahashi et al., 1996; Nath et al., 2000; Thompson et al., 2004; Mattson et al., 2005; Rumbaugh and Nath, 2006). During the course of infiltration of HIV-1–infected monocytes/macrophages into the CNS, macrophages, and microglia provide the brain reservoir of the virus (Nath et al., 2000; Bruce-Keller et al., 2003; Catani et al., 2003). The viral toxins that are released from HIV-1–infected cells are present extracellularly in the HIV-1-infected brain. One of the viral products that is released by HIV-1–infected cells is the transactivator of transcription (Tat) (Bansal et al., 2000; Nath et al., 2000; Catani et al., 2003). The nonstructural protein Tat is a likely agent of the observed neuronal loss in HIV-1–infected patients and has been detected in the brain of patients with AIDS (Jones et al., 2000; Valle et al., 2000). Tat has been studied extensively in *in vitro* and *in vivo* studies (Cheng et al., 1998; Bansal et al., 2000; Bruce-Keller et al., 2003; Fitting et al., 2008a, Maragos et al., 2003; Singh et al., 2004; Aksenov et al., 2001, 2003, 2006; Aksenova et al., 2005, 2006). Tat exposure in rats produces a similar pattern of neuronal damage as seen in patients with HIV-1 encephalitis suggesting that Tat is a causative pathophysiological agent in HIV-1 encephalitis (Maragos et al., 2003).

Tat is reported to be released from productively infected cells, such as macrophages/microglia, and interacts extracellularly with different cell membrane-associated receptors that trigger signal transduction pathways (Brigati et al., 2003). Extracellular Tat induces

neurotoxicity in the CNS by promoting the production of cytokines/chemokines and the expression of cytokine/chemokine receptors (Nath et al., 1999; Brigati et al., 2003). Extracellular Tat is also taken up and internalized by neuronal cells and localized in the nucleus (Ma and Nath, 1997). Further, it has been demonstrated that Tat induces Ca^{2+} desensitivity of neurons (Cheng et al., 1998) and neuronal cell death (Pocernich et al., 2005).

By using extant preclinical models, such as transgenic rats/ mice or direct CNS injection of the virotoxins, it is possible to study the direct effects of the HIV-1 proteins independent of any secondary HIV-1 infections or the virus per se. Previous *in vivo* studies have established that Tat produces adverse effects on cognitive processes as well as on the pathology of the brain (Bansal et al., 2000; Li et al. 2004; Fitting et al., 2006, 2008a, 2008b). A recent design-based stereology study examined the long-term impact of Tat-induced neurotoxicity on the anatomy of the hippocampus in adult rats following intrahippocampal injection on postnatal day (P)1 (Fitting et al., 2008a). Neonatal Tat exposure caused selective neuronal loss in the cornu ammonis fields (CA) (CA)2/3 and hilus of the dentate gyrus (DGH), paralleling findings of a human study reporting a selective vulnerability of CA3 hippocampal neurons to AIDS-related injury (Petito et al., 2001). Tat also increased the estimated total number of astrocytes and oligodendrocytes. Additional results suggested that the effects on cell number in the DGH were predictive of the spatial memory alterations observed in adulthood (Fitting et al., 2008b). Collectively, these findings strongly support the hypothesis that Tat plays a significant role in pediatric HIV-1 neuropathogenesis and the development of psychological impairments that are reported in children infected with HIV-1.

The variable onset and rate of progression of the CNS disease in the pediatric HIV-1 population is not well understood. Clinical studies suggest that different rates of disease progression may relate to the viral load of the mother and/or child, strain of HIV, maternal HIV-1 disease stage, genetic vulnerabilities, and timing of perinatal infection (Belman, 1997; Chearskul et al., 2002). Preclinical studies investigating the effects of P10 Tat exposure in comparison to those reported following P1 Tat exposure (Fitting et al., 2008a,b), will provide critical data on the relative importance that timing may play in vertical transmission. Most of the human pediatric HIV/AIDS cases are reported as “occurring in the period shortly before and after birth, variously defined as beginning with completion of the 20–28th week of gestation and ending 7–28 days after birth” and thus have not clearly distinguished timing of infection (Wiley et al., 1994).

The goal of the present study was to determine the dose-dependent long-term impact of Tat on the adult hippocampus following intrahippocampal injection on P10. From the point of view of brain development, the peak in the rate of brain growth in humans occurs at birth and is also the time when MTCT is putatively held to occur most frequently (Kourtis et al., 2001). The peak in the rate of brain growth in rats occurs at approximately P10 and thus models clinical HIV-1 CNS infection at labor/delivery. In contrast, rat P1 exposure, as previously reported (Fitting et al., 2006; 2008a,b) preceded the marked postnatal increase in the rate of brain growth and thus, modeled clinical HIV-1 CNS infection *in utero*.

Using the same design-based stereology procedure as previously employed (Fitting et al., 2008a), unbiased stereological estimates were used to quantify total neuron number (Nissl stain) in the five major subregions of the rat hippocampus: granular layer (GL), DGH, CA2/3, CA1, and SUB. Glial cells (astrocytes and oligodendrocytes) were quantified in the DGH and the SUB. For each cell type, estimates of cell area and cell volume were taken in the DGH to determine potential alterations in cell morphology. The present study also incorporated a dose-response design to more critically determine the contribution of late Tat exposure to the pathological impairments noted within the pediatric HIV-1 population. Further, in conjunction with the recent reports of the effects of P1 Tat exposure (Fitting et

al., 2008a), the findings of the present study were anticipated to provide a better understanding of timing of infection as a factor explaining the variance of rate of progression of pediatric HIV-1 CNS infection.

MATERIALS AND METHODS

Animals

Pregnant Sprague-Dawley female rats ($N = 8$) were obtained from Harlan Laboratories (Indianapolis, IN) and delivered to the vivarium before Embryonic Day 7. Dams were housed singly with food (Pro-Lab Rat, Mouse Hamster Chow #3,000, NIH diet #31) and water available ad libitum. The animal facility was maintained at 20 ± 2°C, 50 ± 10% relative humidity and was kept on a 12 h light: 12 h-dark cycle with lights on at 07:00 h (EST). The day pups were found in the cage was designated as P0. On P10, male pups from each litter were randomly assigned to each of the four specific treatment conditions. Animals were tested in multiple behavioral tests throughout development starting at P13 and lasting until adulthood (unpublished observations). No evidence of any type of tumors, cataracts, or other gross pathology was found in the animals at the time of sacrifice. At 154–160 days of age (~5 months of age) animals were sacrificed and five animals of each group were randomly chosen by an investigator, naive to treatment condition, to be used for histological studies. The experimental protocol was approved by the Institutional Animal Care and Use Committee (IACUC) at the University of South Carolina, Columbia. Animals were maintained according to National Institute for Health (NIH) guidelines in American Association for Accreditation of Laboratory Animal Care (AAALAC) accredited facilities.

Surgical Techniques and Protein Treatment

Standard stereotaxic surgery techniques, modified for neonates, were used for treatment injection. Direct CNS injection models the acute exposure of the CNS to the virotoxin; vertical transmission of HIV-1 occurs at labor/delivery. Individual pups at P10 were removed from the dam. Sevoflurane (Abbott Laboratories, North Chicago, IL) in 3% oxygen was used as an inhalation anesthetic and pups were then placed in a modified stereotaxic holder for surgery of neonates (David Kopf Instruments, Tujunga, CA). During surgery the pup inhaled sevoflurane through a nose cone and was kept in an anesthetized state until surgery was finished. Body temperature was maintained at 37°C with a heating pad. Rubber head bars held the skull in place while bilateral microinjection was made directly into the hippocampus using stereotaxic coordinates and a microsyringe (Hamilton Co., Reno, NV). The set of coordinates used for the left and right hippocampus were 2.3 mm posterior to the bregma, ±1.0 mm lateral to bregma, −2.5 mm dorsal from dura. Pilot work with Nissl-stained sections through the hippocampus confirmed the injection coordinates for the experimental protocol. An injection volume of 2.0 μl was released over two min after a 1-min resting period that allowed the tissue to return to its original conformation. Animals were bilaterally injected with one of the four treatment conditions: sterile buffer [vehicle (VEH); 10 mM Tris HCl, 300 nM NaCl, pH = 7.58, sterile)], 5 μg Tat, 25 μg Tat, or 50 μg Tat. For the Tat treatment condition, a commercially available recombinant biologically active full-length $Tat_{1–86}$ was purchased (Diatheva s.r.l., Italy). The doses used in the present study bracketed the Tat dose that was recently reported (Fitting et al., 2008a). The injection needle was withdrawn over 2 min to prevent reflux. The piercings in the skin of the head were closed with surgical glue and surgical polypropylene suture (Ethicon, Inc., Johnson & Johnson Health Care Systems, Piscataway, NJ). Pups were placed in a chamber on a heating pad (37°C) for recovery from the anesthesia, before being returned to the dam, where they were closely observed for any indications of rejection. No pup was rejected or abused by the dam.

Stereology

Tissue processing, sectioning, cresyl violet staining, and mounting, as well as the definition of the five subregions of the hippocampus and the identification criteria of the different cell types, followed the protocols as reported recently (Fitting et al., 2008a). Briefly, fixed, blocked brain tissue containing the entire hippocampus was sectioned into 50 μm thick slices in the transverse/horizontal plane with a microtome cryostat (Microm HM500M, Walldorf, Germany). Using the free-floating technique, ~110–130 consecutive sections were collected throughout the hippocampus from each animal. Every 6th section in the series (systematic-randomly sampling) was cresyl violet (Nissl) stained [1 g cresyl violet acetate (Sigma, St. Louis, MO) in 400 ml distilled water (pH 4.0)]. Tissue shrinkage was accompanied during the course of tissue preparation that reduced the z-axis to an average weighted section thickness of ~18 μm.

The five hippocampal cellular layers used in the present study included the GL, hilus of the DGH, cornu ammonis fields 2/3, CA1, and subiculum (SUB). For purposes of stereological quantification, the boundaries of the five cellular layers were defined at all levels of each section series consistently across subjects based on morphologic appearance and clearly identifiable cytoarchitectural landmarks. The five hippocampal areas that were manually outlined are illustrated in a horizontal section of the hippocampus in Figure 1. Visual identification and manual counting of the different cell types was conducted throughout the predefined disector height of the tissue section. Neurons in each of the five subregions were identified morphologically by their larger, pale nuclei surrounded by darkly stained cytoplasm containing Nissl bodies. For all five subregions only cell types with a clearly definable nucleus were included in this study. For the DGH and the SUB, additionally, astrocytes and oligodendrocytes were identified and counted (Fig. 2). Astrocytes were identified from neuronal counts by their relatively smaller size (10 μm in diameter), smaller nucleus (oval pale nucleus), and lack of stained cytoplasm (solid white arrowhead in Fig. 2). On the other hand, oligodendrocytes are smaller (7 μm in diameter) than astrocytes, are somewhat box-like or pear-shaped, and usually appear in clumps or rows (solid black arrowhead in Fig. 2). Compared to astrocytes, their round, eccentric nuclei are smaller, darker, and more densely packed with chromatin (Dodd, 1979).

For stereology, the same imaging system [Nikon eclipse E800 microscope (Nikon, Melville, NY) equipped with a motorized LEP MAC 5,000 XYZ stage controller (Ludl Electronic Products, NY); StereoInvestigator software 7.0 (Microbrightfield, Williston, VT)] and the same stereology estimates, i.e., optical fractionator and the nucleator, were used (see Fitting et al., 2008a). The optical fractionator was used as a stereological technique to obtain unbiased estimates of total number of neurons, astrocytes, and oligodendrocytes (West et al., 1991; Gundersen et al., 1999). The nucleator probe was used within the context of the optical fractionator to estimate the mean cross-sectional cell volume of neurons, astrocytes, and oligodendrocytes in the DGH.

The sampling scheme for the optical fractionator that was used to count cells in a known fraction in the five different hippocampal subregions is presented in Table 1. The number of each cell type (C) in each of the subregions is estimated as:

$$C = \sum Q^{-} * t/h * 1/\mathrm{asf} * 1/\mathrm{ssf} \quad (1)$$

where ΣQ^{-} is the total number of cells counted in the disectors that fell within the sectional profiles of the subregion seen on the sampled sections, t is the section thickness, h is a known fraction of the section thickness that is measured by the optical disector height, asf is the areal sampling fraction calculated by the area of the counting frame of the disector that was overlaid on the area of interest in a random manner, a(frame) and the area associated

with each *x, y* movement, grid(*x, y* step) {asf = [*a*(frame)/*a*(*x, y* step)]}, and ssf is the fraction of the sections sampled or section sampling fraction. On the basis of previous studies, ssf is 1/12 and refers to the smoothness in the data from one section to the other (West et al., 1991; Slomianka and West, 2005). Thus, a sample from a known fraction of the entire hippocampus (fractionator sampling) is generated by the counts with the disectors and can be used to get an estimate of the total number of each cell type (West et al., 1991).

The procedures for sampling with the optical disector as well as the nucleator followed the description as presented in Fitting et al. (2008a). Briefly, areas of the five subregions were outlined on one side of the hippocampus per animal. Counts and volume estimates were performed using a 100× oil immersion objective [Nikon Plan Apo TRIF, 100×/1.45 oil (N.A.), DIC H ∝/0.17WD, 0.13; resulting in a field of view on the monitor that was 110 × 85 μm]. Section thickness was measured before counting started for each grid site. The number of nuclei were counted with unbiased counting rules and a counting frame that was focused through the *h* depth of the section thickness (West et al., 1991). All data in this study were collected by investigators blind to animal treatment. The nucleator was used during the process of counting the cells in the DGH, thus, within the context of the optical fractionator. Estimates of cell volume were generated by using four equally spaced radial lines that extended out from the central reference point. The reference point was chosen to be the middle of each cell type. Estimations of the average cell volume for the three cell types were conducted by marking the intersection of each radial line with the boundary of the cell, thus measuring cell volume of each sampled cell.

RESULTS

Data Analysis

All data were analyzed using analysis of variance (ANOVA) techniques (SPSS 2005, Version 14.0 for Windows, SPSS, Chicago, IL) and summarized in figures, tables, and text as mean (±SEM). One-way ANOVAs with Tat treatment (4 levels: VEH, 5 μg Tat, 25 μg Tat, 50 μg Tat) as a between-subjects factor were conducted for estimates of cell number and cell volume. Specific planned contrasts were used, (1) comparing the VEH group with the Tat dose groups (overall treatment effect), (2) performing orthogonal component analyses to determine specific dose-dependent treatment effects for Tat (dose-dependent treatment effect), and (3) comparing VEH-treated animals with each of the three treatment conditions for Tat (threshold effect; using the Dunnett correction factor, one-tailed). For the DGH and the SUB, data were further analyzed by two-way mixed model ANOVAs, with cell type as a within-subjects factor [Tat (4 levels) × cell type (3 levels: neurons, astrocytes, oligodendrocytes)]. For the within-subjects term (i.e., cell type), potential violations of sphericity (Winer, 1971) were preferentially handled by the use of orthogonal decomposition or, if necessary, the use of the Greenhouse-Geisser df correction factor (Greenhouse and Geisser, 1959). An alpha level of $P \leq 0.05$ was considered significant for all statistical tests used.

Cell Number in the Different Hippocampal Subregions (Optical Fractionator)

Estimates of cell number in the five subregions of the hippocampus, the GL, DGH, CA2/3, CA1, and SUB, are presented in Table 2 and Figure 3, along with the coefficients of error [CE, calculated using the formula by (Gundersen et al., 1999)] and the results of the one-way ANOVAs.

Estimated total number of neurons was not affected by Tat treatment. Planned contrast analyses for Tat treatment revealed no overall treatment effect and no dose-dependent treatment effect.

Separate two-way mixed model ANOVAs (Tat × cell type) were conducted on the DGH and the SUB (Fig. 4).

Cell numbers for the DGH are illustrated in Figure 4A. A significant cell type effect was noted [$F(2, 32) = 65.4$, $P_{GG} \leq 0.001$], with neurons < astrocytes < oligodendrocytes. Analyses for astrocytes revealed a significant Tat effect (Table 2). Analyses of the three basic questions revealed (1) a significant overall treatment effect [$F(1, 16) = 6.9$, $P \leq 0.05$] with (2) a linear dose-response component [$F(1, 16) = 9.5$, $P \leq 0.01$] (Fig. 4A). Planned comparisons revealed (3) a significant increase of the estimated total number of astrocytes for the 50 μg Tat dose condition compared to the VEH-treated group ($P \leq .01$) (Fig. 4A). For the oligodendrocytes, analyses of the three basic questions revealed (1) a significant overall treatment effect [$F(1, 16) = 5.4$, $P \leq 0.05$], (2) a dose-response effect with a linear Tat dose-dependent increase [$F(1, 16) = 4.7$, $P \leq .05$], and (3) a significant increase of the estimated total number of oligodendrocytes for the 50-μg Tat dose condition compared to the VEH-treated group ($P \leq 0.05$).

Cell numbers for the SUB are illustrated in Figure 4B. A significant main effect for cell type was revealed [$F(2, 32) = 350.5$, $P_{GG} \leq 0.001$]. Analyses for astrocytes revealed a significant Tat effect (Table 2). Analyses of the three basic questions revealed (1) a significant overall treatment effect [$F(1, 16) = 10.9$, $P \leq 0.01$] and (2) a linear dose-response component [$F(1, 16) = 11.9$, $P \leq 0.01$] (Fig. 4B). (3) Planned comparisons revealed significant increases of the estimated total number of astrocytes for the 25 μg Tat dose condition compared to the VEH-treated group ($P \leq 0.05$) and the 50 μg Tat dose condition compared to the VEH-treated group ($P \leq 0.01$) (Fig. 4B). For the oligodendrocytes in the SUB, no effects were noted as statistically significant.

Cell Volume (Nucleator)

A two-way mixed model ANOVA (Tat × Cell Type) was conducted on cell morphology in the DGH, i.e., cell volume (Fig. 5).

A significant cell type effect was noted, $F(2, 32) = 410.8$, $P_{GG} \leq 0.001$, neurons (M ± SEM, 2039.0 ± 102.1) > astrocytes (260.3 ± 11.6) > oligodendrocytes (74.9 ± 2.8). Analyses for neurons revealed (1) no significant overall treatment effect, (2) a dose-response effect that approximates a linear relationship [$F(1, 16) = 3.6$, $P \leq 0.07$], and (3) a significant decrease of the estimated cell volume for the 25 μg Tat dose condition compared to the VEH-treated group ($P \leq 0.05$). For the astrocytes and oligodendrocytes, the three basic questions were examined and revealed no overall treatment effect and/or dose-response effect.

DISCUSSION

The present stereology study provided evidence for a long-term dose-response effect of Tat exposure (5–50 μg) on glial cells when injected on P10. A linear dose-dependent increase in the number of astrocytes in the DGH and SUB as well as the number of oligodendrocytes in the DGH was observed. The effects observed following 50 μg Tat dose treatment appeared similar to the effects induced by a Tat exposure dose of 25 μg on P1 (Fitting et al., 2008a). In contrast, estimates of the total number of neurons were not affected by Tat treatment, whereas neuronal loss was demonstrated in the DGH and the CA2/3 region by 25 μg Tat on P1 (Fitting et al., 2008a). The viral exposure animal model suggests that the developing CNS system appears to be most vulnerable early in development at a time point that precedes the marked postnatal increase in rate of brain growth.

The anatomical parameters of the present study were based on a design-based stereology technique, the optical fractionator that by definition yields unbiased estimates of population

number (West et al., 1991). By using the fractionator in combination with the optical disector samples, estimates of *N* are unaffected by shrinkage before and after preparation of the sections. It also eliminates the problem of lost caps because the disector is positioned 2 μm below the upper surface of the section and counting is performed through a depth of 10 μm, leaving the remaining thickness at the bottom of the section. Further, the optical fractionator does not require rigorous definitions of structural boundaries, which is otherwise an important attribute in estimating the total number of cells when using the optical disector as a technique. Thus, the cell count measure provided an account estimation of true cell number.

Estimates of the total neuron number in each of the five subregions of the hippocampus in the vehicle control group are comparable with findings reported in other studies that used the optical fractionator (e.g., West et al., 1991; Rapp and Gallagher, 1996; Lister et al., 2005; Fitting et al., 2008a). As is illustrated in Table 3, the estimates well approximate each other, with the small differences perhaps being attributable to the diversity of strains and ages of the animals being used by the various investigators.

Regarding the long-term effects of Tat when administered on P10, the doses of Tat used (5–50 μg) did not induce any significant effects on the estimated total number of neurons. In contrast, when 25 μg Tat was injected on P1 (Fitting et al., 2008a) a significant decrease in the number of neurons in the DGH and the CA2/3 region was noted. Given that the highest dose of Tat in the present study was twice as high as the dose used in the previous P1 stereology study (Fitting et al., 2008a), it is suggested that Tat exposure during the period before postnatal increase in the rate of brain growth (injection of Tat on P1) is more vulnerable to neuronal cells than exposure of Tat on P10, which approximates the peak in the rats' rate of brain growth. However, note that animals in the P1 study were sacrificed at ~7[1/2] months of age, whereas animals in the present study were sacrificed earlier at ~5 months of age (Fitting et al., 2008a). Future studies should also examine whether the additional length of the post-Tat exposure period may be a contributing factor to neuronal loss.

Regarding the supporting glial cells, the estimated total number of astrocytes was dose dependently increased by Tat in DGH and SUB. For oligodendrocytes, a dose-dependent increase in total number was also noted in the DGH. The finding of an increase in number of astrocytes and oligodendrocytes is supported by the previous stereology P1 study (Fitting et al., 2008a). It should be noted that future studies using specific immunohistochemical techniques for glia subtypes might be helpful to confirm the morphological distinctions made between astrocytes and oligodendrocytes.

Comparing estimates of the total number of glial cells following P1 vs. P10 administration of the same dose of Tat, i.e., 25 μg, revealed differential effects in the DGH and SUB across the two studies. When injected on P1, estimates of numbers of astrocytes and oligodendrocytes in the DGH appeared to be twice as great as when injected on P10, i.e., 25 μg of Tat in the P1 study increased astrocytes by 90% relative to VEH-treated animals, whereas when injected on P10 (present study) the number of astrocytes was increased by only ~40%compared to the VEH-treated animals. In contrast, for the SUB, across both the P1 and P10 injection times, the number of astrocytes and oligodendrocytes was increased by ~65%and 23–26%, respectively, relative to their VEH-treated animals. In the light of the findings on glial cells, it again supports the suggestion that the developing CNS system appears to be more vulnerable early in development prior to the postnatal increase in the rate of brain growth. In general, however, the number of cells in the SUB was higher in the P10 vs. P1 study (for neurons it was ~25% for astrocytes it was ~87% for oligodendrocytes it was ~24%) which however cannot be attributed to viral protein P10 exposure, because it

was also found in the vehicle control group (for neurons it was ~20%, for astrocytes it was ~93%,for oligodendrocytes it was ~16%). Time of injection (P1 vs. P10) might have significantly contributed to the observed differences. Importantly, it should be noted that the reported pattern of estimates of the total number of neurons and glial cells in the DGH and SUB of the previous study (Fitting et al. 2008a) was replicated in the present dose-response study (Fig. 4).

It is reported that, unlike astrocytes that appear to react to injury to promote recovery, oligodendrocytes have a more passive role and are more easily damaged as a general response to insults (Yong, 1998). With respect to extrinsic determinants, astrocytes have significant influence on the behavior of oligodendrocytes (Yong, 1998). Astrocytes appear to have a protective mechanism of oligodendrocytes and affect the proliferation of oligodendrocyte precursors (McLaurin and Yong, 1995). The finding of an increased number of astrocytes by Tat exposure is parallel to human studies where astrogliosis is frequently reported in pediatric HIV-1 infection (Saito et al., 1994; Tornatore et al., 1994; Vallat et al., 1998). It is suggested that astrocyte infection is more frequent in children than in adults (Vallat et al., 1998) and contributes significantly to HIV-1 neuropathogenesis (Saito et al., 1994). Pathologic tissues of children who died with AIDS encephalopathy (postmortem pediatric CNS tissues) have shown a latent and nonproductive HIV-1 infection of astrocytes, indicated by the expression of HIV-1 gene products in up to 20% of astrocytes (Saito et al., 1994; Tornatore et al., 1994). Astrocytes have recently been demonstrated to be able to modulate CNS neuronal synapses, and consequently, information processing in the brain (Nadkarni and Jung, 2004; Perea and Araque, 2005). Further, they are responsible for maintaining an optimal microenvironment for neurons, and the finding of an increased estimated total number of astrocytes might suggest an attempt to promote regeneration after HIV-1 Tat protein-induced neurotoxicity. The increased estimated total number of astrocytes after injury is supported by a previous study that evaluated reactive gliosis in autopsy hippocampus of patients with AIDS (Petito et al., 2001). The authors report an increased number of hippocampal GFAP-positive astrocytes and LN3-positive microglia in patients with AIDS with HIV.

Regarding the cell morphology in the DGH, the present dose-response study demonstrated an effect of Tat on neuron cell volume. The dose-response function was best characterized by an approximate linear relationship; however, pairwise comparisons to control, only confirmed the 25 μg Tat dose group as significantly decreasing neuronal cell volume from controls. No effect was statistically detected for astrocytes or oligodendrocytes. No significant effect of Tat on cell morphology of neurons, astrocytes, or oligodendrocytes was reported following P1 Tat exposure (Fitting et al., 2008a), suggesting that long-term effects of viral proteins were not necessarily determined by an alteration in cell morphology. Future studies are necessary to further explore the effect of P10 Tat exposure on cell morphology. Further, it should be acknowledged that the nucleator method provides unbiased estimates of cell volume provided the isotropy requirement is met. Particularly with the bipolar orientation of the pyramidal cell layer, we are not able to ensure the condition of isotropy was met.

Collectively, the findings of the present study, in combination with the previous stereology-based P1 study, suggest that neonatal Tat exposure that precedes the marked postnatal increase in rate of brain growth may be more damaging to the developing CNS compared to P10 Tat exposure, that approximates the peak in the rats' rate of brain growth. The potential translational relevance of this main preclinical finding to humans (based on human brain growth rate) suggests that early clinical HIV-1 CNS infection *in utero* would be more deleterious to the developing CNS relative to HIV-1 CNS infection that occurs during labor or delivery. It is suggested that the factor of timing of infection plays a crucial role in

distinguishing infants with rapid disease progression from those with slower disease progression, i.e., children infected with HIV early in life being more vulnerable to CNS disease. Variability in the progression of pediatric HIV/AIDS may therefore be better understood with the knowledge of timing of HIV-1 CNS infection.

Acknowledgments

Grant sponsor: National Institute on Drug Abuse; Grant numbers: DA013137, DA014401; Grant sponsor: National Institute of Child Health and Human Development; Grant number: HD043680

REFERENCES

Aksenova MV, Aksenov MY, Mactutus CF, Booze RM. Cell culture models of oxidative stress and injury in the central nervous system. Curr Neurovasc Res. 2005; 2:73–89. [PubMed: 16181101]

Aksenova MV, Silvers JM, Aksenov MY, Nath A, Ray PD, Mactutus CF, Booze RM. HIV-1 Tat neurotoxicity in primary cultures of rat midbrain fetal neurons: Changes in dopamine transporter binding and immunoreactivity. Neurosci Lett. 2006; 395:235–239. [PubMed: 16356633]

Aksenov MY, Hasselrot U, Bansal AK, Wu G, Nath A, Anderson C, Mactutus CF, Booze RM. Oxidative damage induced by the injection of HIV-1 Tat protein in the rat striatum. Neurosci Lett. 2001; 305:5–8. [PubMed: 11356294]

Aksenov MY, Hasselrot U, Wu G, Nath A, Anderson C, Mactutus CF, Booze RM. Temporal relationships between HIV-1 Tat-induced neuronal degeneration, OX-42 immunoreactivity, reactive astrocytosis, and protein oxidation in the rat striatum. Brain Res. 2003; 987:1–9. [PubMed: 14499939]

Aksenov MY, Aksenova MV, Nath A, Ray PD, Mactutus CF, Booze RM. Cocaine-mediated enhancement of Tat toxicity in rat hippocampal cell cultures: The role of oxidative stress and D1 dopamine receptor. Neurotoxicology. 2006; 27:217–228. [PubMed: 16386305]

Annunziata P. Blood-brain barrier changes during invasion of the central nervous system by HIV-1. Old and new insights into the mechanism. J Neurol. 2003; 250:901–906. [PubMed: 12928906]

Bansal AK, Mactutus CF, Nath A, Maragos W, Hauser KF, Booze RM. Neurotoxicity of HIV-1 proteins gp120 and Tat in the rat striatum. Brain Res. 2000; 879:42–49. [PubMed: 11011004]

Belman, AL. Infants, children, and adolescents. In: Berger, JR.; Levy, RM., editors. AIDS and the Nervous System. 2nd ed.. Philadelphia: Lippincott-Raven; 1997. p. 223-253.

Blanche S, Tardieu M, Duliege A, Rouzioux C, Le Deist F, Fukunaga K, Caniglia M, Jacomet C, Messiah A, Griscelli C. Longitudinal study of 94 symptomatic infants with perinatally acquired human immunodeficiency virus infection. Evidence for a bimodal expression of clinical and biological symptoms. AMA Am J Dis Child. 1990; 144:1210–1215.

Brigati C, Giacca M, Noonan DM, Albini A. HIV Tat, its TARgets and the control of viral gene expression. FEMS Microbiol Lett. 2003; 220:57–65. [PubMed: 12644228]

Bruce-Keller AJ, Chauhan A, Dimayuga FO, Gee J, Keller JN, Nath A. Synaptic transport of human immunodeficiency virus-Tat protein causes neurotoxicity and gliosis in rat brain. J Neurosci. 2003; 23:8417–8422. [PubMed: 12968004]

Catani MV, Corasaniti MT, Ranalli M, Amantea D, Litovchick A, Lapidot A, Melino G. The Tat antagonist neomycin B hexaarginine conjugate inhibits gp-120-induced death of human neuroblastoma cells. J Neurochem. 2003; 84:1237–1245. [PubMed: 12614324]

Chearskul S, Chotpitayasunondh T, Simonds RJ, Wanprapar N, Waranawat N, Punpanich W, Chokephaibulkit K, Mock PA, Neeyapun K, Jetsawang B, Teeraratkul A, Supapol W, Mastro TD, Shaffer N. Bangkok Collaborative Perinatal HIV Transmission Study Group Survival, disease manifestations, and early predictors of disease progression among children with perinatal human immunodeficiency virus infection in Thailand. Pediatrics. 2002; 110(2 Pt 1):e25. [PubMed: 12165624]

Cheng J, Nath A, Knudsen B, Hochman S, Geiger JD, Ma M, Magnuson DS. Neuronal excitatory properties of human immunodeficiency virus type 1 Tat protein. Neuroscience. 1998; 82:97–106. [PubMed: 9483506]

Dodd, EE. Atlas of Histology. New York: McGraw-Hill Inc; 1979.

Epstein LG, Sharer LR, Oleske JM, Connor EM, Goudsmit J, Bagdon L, Robert-Guroff M, Koenigsberger MR. Neurologic manifestations of human immunodeficiency virus infection in children. Pediatrics. 1986; 78:678–687. [PubMed: 2429248]

Equils O, Garratty E, Wei LS, Plaeger S, Tapia M, Deville J, Krogstad P, Sim MS, Nielsen K, Bryson YJ. Recovery of replication-competent virus from CD4 T cell reservoirs and change in coreceptor use in human immunodeficiency virus type 1-infected children responding to highly active antiretroviral therapy. J Infect Dis. 2000; 182:751–757. [PubMed: 10950768]

Fitting S, Booze RM, Mactutus CF. Neonatal hippocampal Tat injections: Developmental effects on prepulse inhibition (PPI) of the auditory startle response. Int J Dev Neurosci. 2006; 24:275–283. [PubMed: 16530999]

Fitting S, Booze RM, Hasselrot U, Mactutus CF. Differential long-term neurotoxicity of HIV-1 proteins in the rat hippocampal formation: A design-based stereological study. Hippocampus. 2008a; 18:135–147. [PubMed: 17924522]

Fitting S, Booze RM, Mactutus CF. Neonatal intrahippocam-pal injection of the HIV-1 proteins gp120 and Tat: Differential effects on behavior and the relationship to stereological hippocam-pal measures. Brain Res. 2008b; 1232:139–154. [PubMed: 18674522]

Fowler MG. Pediatric HIV infection: neurologic and neuropsychologic findings. Acta Paediatr Suppl. 1994; 400:59–62. [PubMed: 7833564]

Gelbard HA, Epstein LG. HIV-1 encephalopathy in children. Curr Opin Pediatr. 1995; 7:655–662. [PubMed: 8776015]

Gelbard HA, James HJ, Sharer LR, Perry SW, Saito Y, Kazee AM, Blumberg BM, Epstein LG. Apoptotic neurons in brains from paediatric patients with HIV-1 encephalitis and progressive encephalopathy. Neuropathol Appl Neurobiol. 1995; 21:208–217. [PubMed: 7477729]

Greenhouse SW, Geisser S. On methods in the analysis of profile data. Psychometrika. 1959; 24:95–112.

Gundersen HJ, Jensen EB, Kieu K, Nielsen J. The efficiency of systematic sampling in stereology–reconsidered. J Microsc. 1999; 193(Pt 3):199–211. [PubMed: 10348656]

James HJ, Sharer LR, Zhang Q, Wang HG, Epstein LG, Reed JC, Gelbard HA. Expression of caspase-3 in brains from paediatric patients with HIV-1 encephalitis. Neuropathol Appl Neurobiol. 1999; 25:380–386. [PubMed: 10564527]

Jones MV, Bell JE, Nath A. Immunolocalization of HIV envelope gp120 in HIV encephalitis with dementia. AIDS. 2000; 14:2709–2713. [PubMed: 11125889]

Kourtis AP, Bulterys M, Nesheim SR, Lee FK. Understanding the timing of HIV transmission from mother to infant. JAMA. 2001; 285:709–712. [PubMed: 11176886]

Krajewski S, James HJ, Ross J, Blumberg BM, Epstein LG, Gendel-man HE, Gummuluru S, Dewhurst S, Sharer LR, Reed JC, Gel-bard HA. Expression of pro- and anti-apoptosis gene products in brains from paediatric patients with HIV-1 encephalitis. Neuropathol Appl Neurobiol. 1997; 23:242–253. [PubMed: 9223134]

Li ST, Matsushita M, Moriwaki A, Saheki Y, Lu YF, Tomizawa K, Wu HY, Terada H, Matsui H. HIV-1 inhibits long-term potentiation and attenuates spatial learning. Ann Neurol. 2004; 55:362–371. [PubMed: 14991814]

Lister JP, Blatt GJ, DeBassio WA, Kemper TL, Tonkiss J, Galler JR, Rosene DL. Effect of prenatal protein malnutrition on numbers of neurons in the principal cell layers of the adult rat hippocampal formation. Hippocampus. 2005; 15:393–403. [PubMed: 15669101]

Ma M, Nath A. Molecular determinants for cellular uptake of Tat protein of human immunodeficiency virus type 1 in brain cells. J Virol. 1997; 71:2495–2499. [PubMed: 9032389]

Maragos WF, Tillman P, Jones M, Bruce-Keller AJ, Roth S, Bell JE, Nath A. Neuronal injury in hippocampus with human immunodeficiency virus transactivating protein, Tat. Neuroscience. 2003; 117:43–53. [PubMed: 12605891]

Mattson MP, Haughey NJ, Nath A. Cell death in HIV dementia. Cell Death Differ. 2005; 12(Suppl 1): 893–904. [PubMed: 15761472]

McLaurin JA, Yong VW. Oligodendrocytes and myelin. Neurol Clin. 1995; 13:23–49. [PubMed: 7739504]

Mintz M. Clinical comparison of adult and pediatric neuro-AIDS. Adv Neuroimmunol. 1994; 4:207–221. [PubMed: 7874389]

Mintz, M. Neurological findings in pediatric HIV/AIDS. Clinical features. In: Gendelman, HE.; Grant, I.; Everall, IP.; Lipton, SA.; Swindells, S., editors. The Neurology of AIDS. 2nd ed.. Oxford: University Press; 2005. p. 639-658.

Nadkarni S, Jung P. Dressed neurons: modeling neural-glial interactions. Phys Biol. 2004; 1:35–41. [PubMed: 16204820]

Nath A, Conant K, Chen P, Scott C, Major EO. Transient exposure to HIV-1 Tat protein results in cytokine production in macrophages and astrocytes. J Biol Chem. 1999; 274:17098–17102. [PubMed: 10358063]

Nath A, Haughey NJ, Jones M, Anderson C, Bell JE, Geiger JD. Synergistic neurotoxicity by human immunodeficiency virus proteins Tat and gp120: protection by memantine. Ann Neurol. 2000; 47:186–194. [PubMed: 10665489]

Ogundele MO, Coulter JB. HIV transmission through breastfeeding: Problems and prevention. Ann Trop Paediatr. 2003; 23:91–106. [PubMed: 12803739]

Perea G, Araque A. Glial calcium signaling and neuron-glia communication. Cell Calcium. 2005; 38:375–382. [PubMed: 16105683]

Petito CK, Roberts B, Cantando JD, Rabinstein A, Duncan R. Hippocampal injury and alterations in neuronal chemokine co-receptor expression in patients with AIDS. J Neuropathol Exp Neurol. 2001; 60:377–385. [PubMed: 11305873]

Pocernich CB, Sultana R, Mohammad-Abdul H, Nath A, Butterfield DA. HIV-dementia, Tat-induced oxidative stress, and antioxidant therapeutic considerations. Brain Res Rev. 2005; 50:14–26. [PubMed: 15890409]

Rapp PR, Gallagher M. Preserved neuron number in the hippocampus of aged rats with spatial learning deficits. Proc Natl Acad Sci USA. 1996; 93:9926–9930. [PubMed: 8790433]

Rumbaugh JA, Nath A. Developments in HIV neuropathogenesis. Curr Pharm Des. 2006; 12:1023–1044. [PubMed: 16515484]

Saito Y, Sharer LR, Epstein LG, Michaels J, Mintz M, Louder M, Golding K, Cvetkovich TA, Blumberg BM. Overexpression of nef as a marker for restricted HIV-1 infection of astrocytes in postmortem pediatric central nervous tissues. Neurology. 1994; 44(3 Pt 1):474–481. [PubMed: 8145918]

Singh IN, Goody RJ, Dean C, Ahmad NM, Lutz SE, Knapp PE, Nath A, Hauser KF. Apoptotic death of striatal neurons induced by human immunodeficiency virus-1 Tat and gp120: Differential involvement of caspase-3 and endonuclease G. J Neurovirol. 2004; 10:141–151. [PubMed: 15204919]

Slomianka L, West MJ. Estimators of the precision of stereological estimates: an example based on the CA1 pyramidal cell layer of rats. Neuroscience. 2005; 136:757–767. [PubMed: 16344149]

Takahashi K, Wesselingh SL, Griffin DE, McArthur JC, Johnson RT, Glass JD. Localization of HIV-1 in human brain using polymerase chain reaction/in situ hybridization and immunocytochemistry. Ann Neurol. 1996; 39:705–711. [PubMed: 8651642]

Thompson KA, Churchill MJ, Gorry PR, Sterjovski J, Oelrichs RB, Wesselingh SL, McLean CA. Astrocyte specific viral strains in HIV dementia. Ann Neurol. 2004; 56:873–877. [PubMed: 15562411]

Tornatore C, Chandra R, Berger JR, Major EO. HIV-1 infection of subcortical astrocytes in the pediatric central nervous system. Neurology. 1994; 44(3 Pt 1):481–487. [PubMed: 8145919]

UNAIDS. AIDS epidemic update: December 2007. Geneva: Joint United Nations Programme on HIV/AIDS (UNAIDS) and World Health Organization (WHO); 2007. p. 50

Valle LD, Croul S, Morgello S, Amini S, Rappaport J, Khalili K. Detection of HIV-1 Tat and JCV capsid protein, VP1, in AIDS brain with progressive multifocal leukoencephalopathy. J Neurovirol. 2000; 6:221–228. [PubMed: 10878711]

Vallat AV, De Girolami U, He J, Mhashilkar A, Marasco W, Shi B, Gray F, Bell J, Keohane C, Smith TW, Gabuzda D. Localization of HIV-1 co-receptors CCR5 and CXCR4 in the brain of children with AIDS. Am J Pathol. 1998; 152:167–178. [PubMed: 9422534]

West MJ, Slomianka L, Gundersen HJ. Unbiased stereological estimation of the total number of neurons in the subdivisions of the rat hippocampus using the optical fractionator. Anat Rec. 1991; 231:482–497. [PubMed: 1793176]

WHO. HIV and infant feeding counseling: a training course; Trainer's guide. Geneva, WHO, Department of Child and Adolescent Health and Development. 2000. p. 230 p

Wiley CA, Belman AL, Dickson DW, Rubinstein A, Nelson JA. Human immunodeficiency virus within the brains of children with AIDS. Clin Neuropathol. 1990; 9:1–6. [PubMed: 2306889]

Wiley CA, Masliah E, Achim CL. Measurement of CNS HIV burden and its association with neurologic damage. Adv Neuroimmunol. 1994; 4:319–325. [PubMed: 7874400]

Winer, BJ. Statistical Principles in Experimental Design. New York: McGraw-Hill; 1971.

Wolters, PL.; Brouwers, P. Evaluation of neurodevelopmental deficits in children with HIV-1 infection. In: Gendelman, HE.; Grant, I.; Everall, IP.; Lipton, SA.; Swindells, S., editors. The Neurology of AIDS. 2nd ed.. Oxford: University Press; 2005. p. 639-658.

Yong VW. Response of astrocytes and oligodendrocytes to injury. Ment Retard Dev Disabil. 1998; 4:193–199.

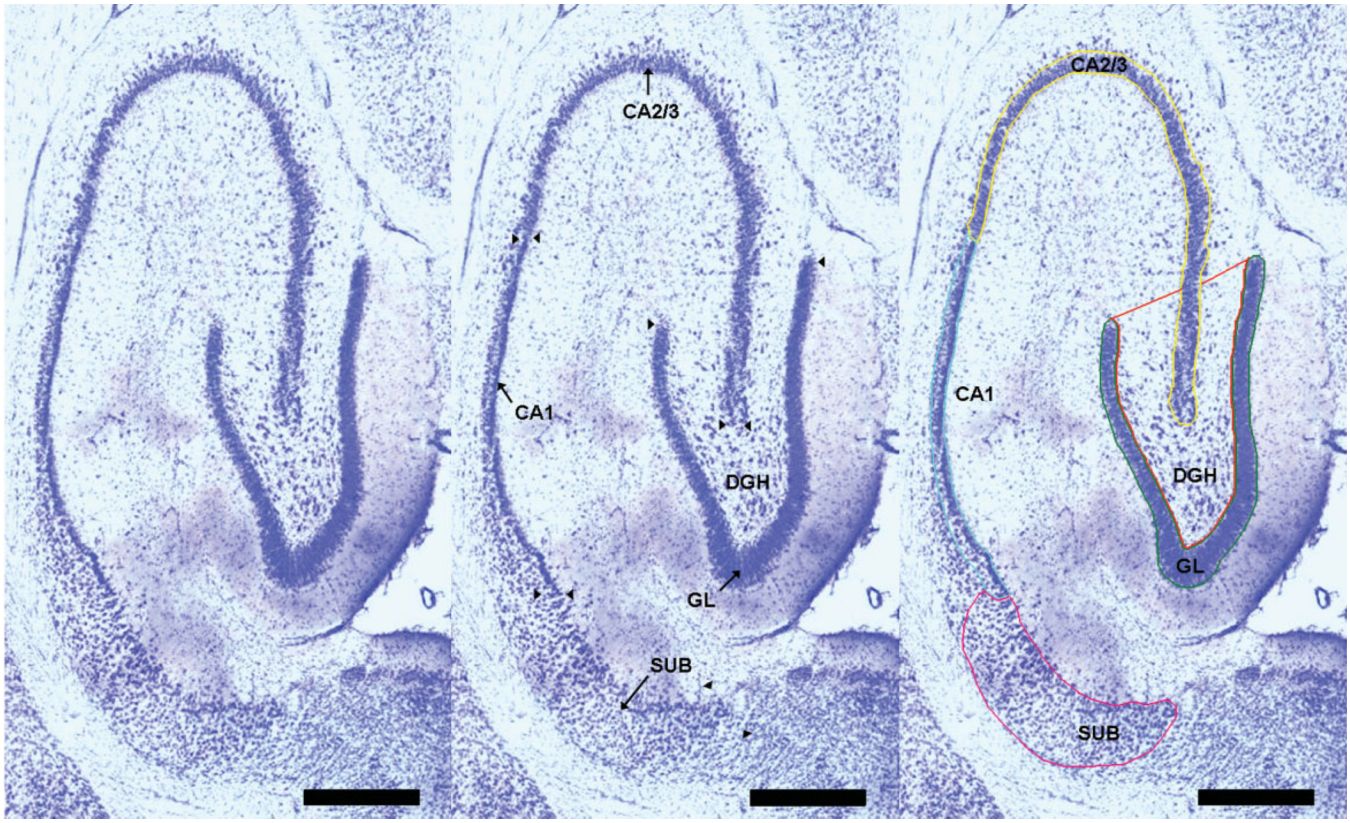

FIGURE 1.

Left Panel: The cytoarchitectonic delineation of hippocampal subfields cut in the horizontal plane. Middle Panel: Arrows indicate the hippocampal subfields for analysis. Arrowheads mark the border between the different hippocampal sub-fields. Right Panel: Boundaries of the cellular layers as outlined on the StereoInvestigator 7.0 system, i.e., the defined regions of interest within cells were counted and cell area and cell volume were taken; Calibration bar = 250 μm, ×4 magnification. [Color figure can be viewed in the online issue, which is available at www.interscience.wiley.com.]

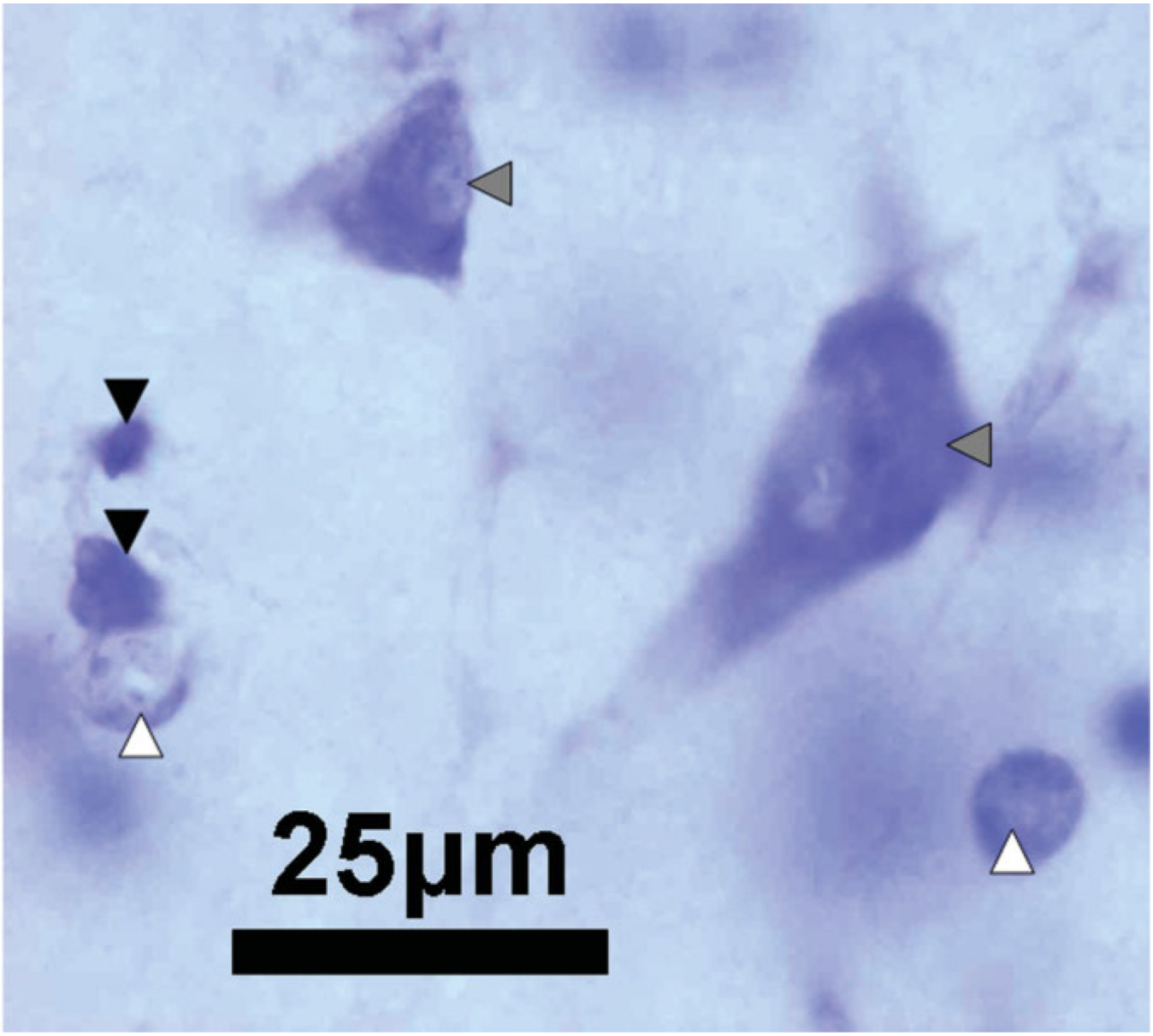

FIGURE 2.

A photomicrograph of the hilus of the dentate gyrus at ×100 magnification, illustrating typical cell types based on morphology and Nissl staining. Neurons, indicated by the solid gray arrowheads, are stained with a large nucleus and a single nucleolus. Astrocytes, indicated by the solid white arrowheads, display pale staining of the nucleus. Oligodendrocytes, indicated by the solid black arrowheads, are identified by dark nuclei; Calibration Bar: 25 µm. [Color figure can be viewed in the online issue, which is available at www.interscience.wiley.com.]

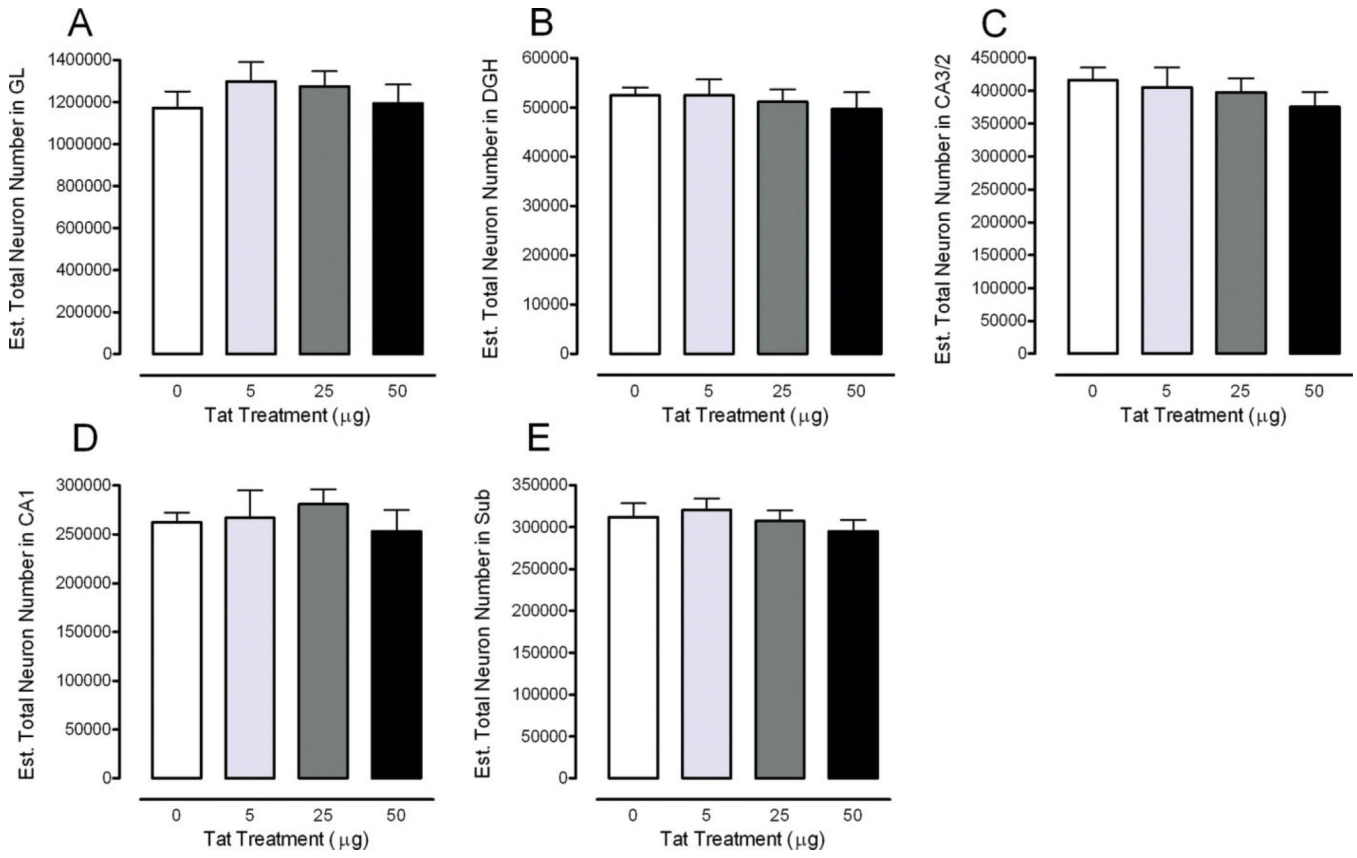

FIGURE 3.

Estimated total number of neurons across the five subregions of the rat hippocampus illustrated as a function of dose of Tat. Region specific illustration of the total neuron number is shown for the (A) granular layer (GL), (B) hilus of the dentate gyrus (DGH), (C) cornu ammonis fields (CA)2/3, (D) CA1, and (E) subiculum (SUB). No significant treatment effects were noted. [Color figure can be viewed in the online issue, which is available at www.interscience.wiley.com.]

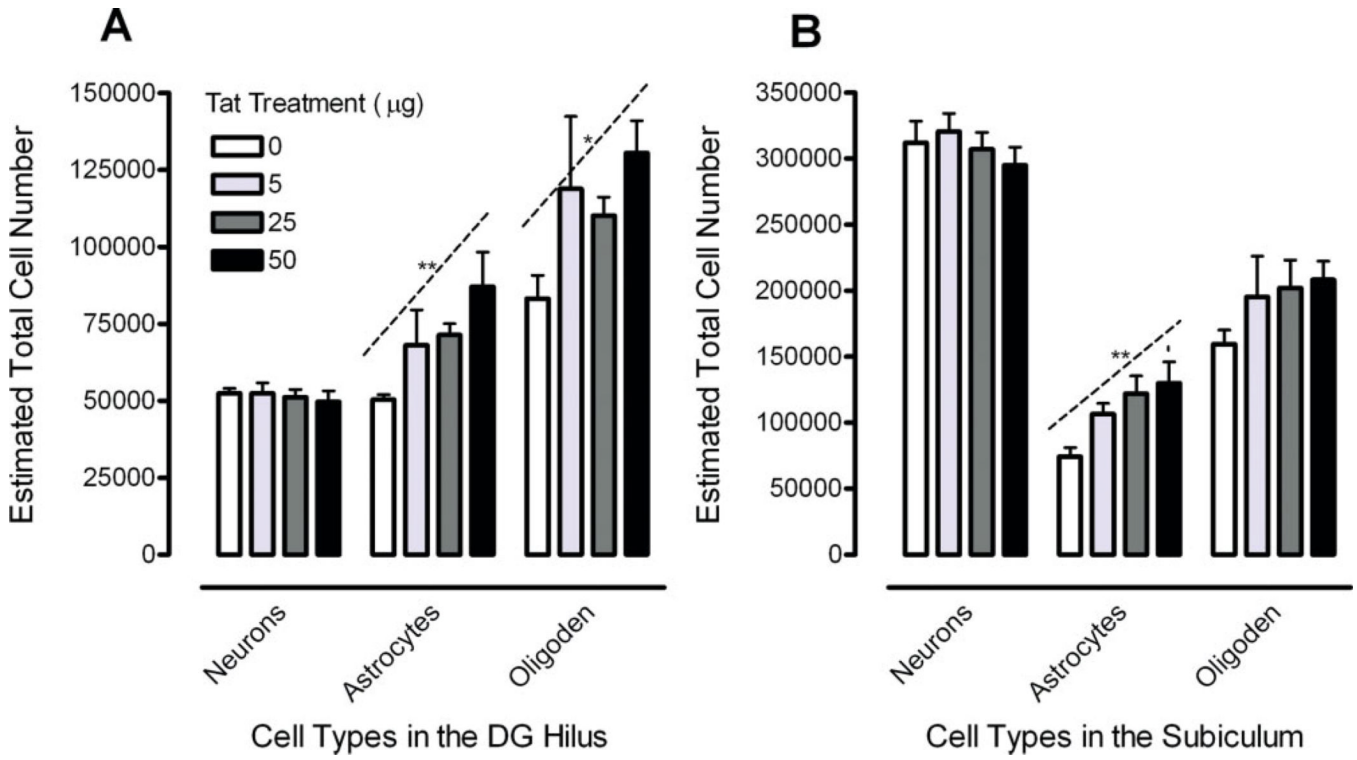

FIGURE 4.

Estimated total number of neurons, astrocytes, and oligodendrocytes illustrated as a function of dose of Tat in the (A) hilus of the dentate gyrus (DGH) with a significant linear Tat dose-response for astrocytes and oligodendrocytes and (B) subiculum (SUB) with a significant linear Tat dose-response for astrocytes, $*P \leq 0.05$; $**P \leq 0.01$. [Color figure can be viewed in the online issue, which is available at www.interscience.wiley.com.]

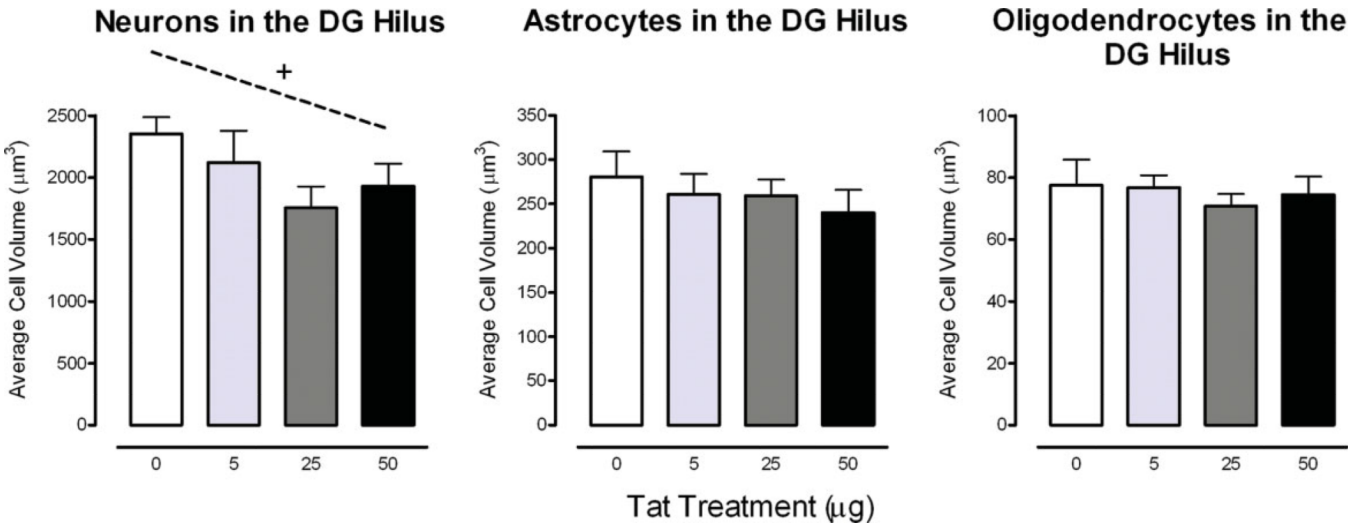

FIGURE 5.

Cell morphology data in the hilus of the dentate gyrus (DGH) illustrated as a function of dose of Tat. Cell volume is displayed with a significant cell type effect. An approximate linear relationship was noted for neurons. $^{+}P \leq 0.08$. [Color figure can be viewed in the online issue, which is available at www.interscience.wiley.com.]

TABLE 1

Fixed Parameters that Describe the Dimensions of the Disector Samples

	Granular layer	DG hilus	CA2/3	CA1	Subiculum
ssf	1/12	1/12	1/12	1/12	1/12
asf: *a*(frame)/grid(*x*, *y* step) (μm^2)					
a(frame) (μm^2)	7×7	35 × 35	13 × 13	15 × 15	25 × 25
grid(*x*, *y* step) (μm^2)	220 × 220	220 × 220	220 × 220	220 × 220	350 × 350
h/*t*[a]					
disect. Ht., h, (μm)	10	10	10	10	10

[a]Section thickness, *t*, varies with each counting frame and is determined during the process of counting.

TABLE 2

Total Number of Cells in the Rat Hippocampus (Unilateral Values) with One-Way ANOVA Result

Litter/Animal	Group	Granular layer Neurons		Neurons		DG Hilus Astrocytes		Oligoden		CA2/3 Neurons		CA1 Neurons		Neurons		Subiculum Astrocytes		Oligoden	
L1/A	VEH	1,388,074	0.08	55,183	0.08	51,377	0.09	110,365	0.06	454,798	0.08	263,128	0.09	306,184	0.08	56,034	0.19	138,083	0.12
L2/A	VEH	1,121,565	0.09	50,990	0.08	49,207	0.09	67,392	0.07	378,672	0.09	249,886	0.09	312,987	0.08	62,597	0.17	142,267	0.12
L3/A	VEH	1,316,016	0.08	56,420	0.08	45,907	0.09	87,258	0.06	450,265	0.08	252,015	0.09	342,139	0.07	89,741	0.14	198,179	0.10
L4/A	VEH	953,549	0.09	52,071	0.08	55,409	0.08	78,774	0.07	434,508	0.07	245,801	0.09	254,138	0.08	86,942	0.14	153,820	0.10
L5/A	VEH	1,082,244	0.09	47,814	0.09	49,908	0.08	72,244	0.07	364,246	0.08	300,074	0.08	345,810	0.07	76,847	0.16	165,220	0.11
Mean *N*(CE)		1,172,290	0.09	52,495	0.08	50,361	0.08	83,207	0.07	416,498	0.08	262,181	0.09	312,252	0.08	74,432	0.16	159,514	0.11
CV			0.15		0.07		0.07		0.20		0.10		0.08		0.12		0.20		0.15
L1/B	Low Tat	1,627,721	0.08	62,820	0.08	107,187	0.06	152,731	0.05	518,297	0.07	375,694	0.08	372,989	0.07	138,144	0.12	307,864	0.08
L2/B	Low Tat	1,304,162	0.08	53,450	0.08	63,612	0.08	193,888	0.06	405,082	0.08	255,532	0.09	293,510	0.08	91,966	0.15	125,231	0.01
L3/B	Low Tat	1,292,784	0.08	52,955	0.08	45,136	0.09	79,966	0.07	395,494	0.08	232,468	0.09	315,387	0.08	99,497	0.01	204,626	0.10
L4/B	Low Tat	1,184,151	0.08	42,359	0.09	77,658	0.06	95,307	0.06	344,459	0.08	221,833	0.09	318,649	0.07	101,836	0.13	164,252	0.10
L5/B	Low Tat	1,083,104	0.09	50,796	0.08	46,273	0.09	72,367	0.07	362,716	0.08	248,698	0.09	303,097	0.08	101,660	0.14	175,081	0.10
Mean *N*(CE)		1,298,384	0.08	52,476	0.08	67,973	0.08	118,852	0.06	405,209	0.08	266,845	0.09	320,726	0.08	106,621	0.11	195,411	0.08
CV			0.16		0.14		0.38		0.44		0.17		0.23		0.10		0.17		0.35
L1/C	Med Tat	1,562,003	0.08	60,609	0.08	66,634	0.07	111,293	0.06	480,626	0.07	309,778	0.08	264,367	0.08	72,929	0.16	164,090	0.11
L2/C	Med Tat	1,153,361	0.09	50,732	0.08	83,474	0.07	130,248	0.05	365,475	0.08	262,541	0.09	313,705	0.08	130,252	0.12	271,511	0.08
L3/C	Med Tat	1,230,082	0.09	47,043	0.09	72,841	0.07	93,328	0.06	371,617	0.09	319,807	0.08	298,847	0.08	116,768	0.13	176,141	0.11
L4/C	Med Tat	1,244,186	0.09	50,324	0.09	61,726	0.08	112,050	0.06	381,275	0.09	273,008	0.09	340,458	0.08	148,563	0.12	169,197	0.11
L5/C	Med Tat	1,180,706	0.09	47,050	0.09	72,296	0.07	104,046	0.06	390,313	0.08	239,045	0.09	319,725	0.08	142,317	0.12	230,046	0.09
Mean *N*(CE)		1,274,068	0.09	51,152	0.09	71,394	0.07	110,193	0.06	397,861	0.08	280,836	0.08	307,420	0.08	122,166	0.13	202,197	0.10
CV			0.13		0.11		0.11		0.12		0.12		0.12		0.09		0.25		0.23
L1/D	High Tat	1,440,265	0.08	61,054	0.07	131,836	0.05	171,756	0.04	433,263	0.08	325,448	0.08	306,390	0.08	175,333	0.10	246,175	0.08
L2/D	High Tat	1,153,244	0.08	54,169	0.08	75,499	0.07	114,094	0.05	366,471	0.08	259,205	0.08	246,033	0.08	88,233	0.14	161,194	0.10
L3/D	High Tat	1,030,920	0.09	44,401	0.09	78,106	0.06	122,831	0.05	325,343	0.09	220,891	0.09	290,303	0.08	159,093	0.10	216,497	0.09
L4/D	High Tat	983,893	0.09	44,358	0.09	75,547	0.07	121,984	0.05	331,125	0.09	197,620	0.10	311,462	0.07	122,176	0.12	216,819	0.09
L5/D	High Tat	1,364,699	0.08	44,672	0.09	74,576	0.07	121,832	0.06	422,830	0.08	261,346	0.09	322,861	0.08	104,510	0.13	201,555	0.10
Mean N (CE)		1,194,604	0.08	49,731	0.08	87,113	0.06	130,499	0.05	375,806	0.08	252,902	0.09	295,410	0.08	129,869	0.12	208,448	0.09
CV			0.17		0.15		0.29		0.18		0.13		0.19		0.10		0.28		0.15

Litter/Animal	Group	Granular layer Neurons	Neurons	DG Hilus Astrocytes	Oligoden	CA2/3 Neurons	CA1 Neurons	Neurons	Subiculum Astrocytes	Oligoden
1-way ANOVA		<1.0	<1.0	3.33	2.15	<10	<1.0	<1.0	4.32	1.13
F(3, 16)										
P value		n.s.	n.s	$P < 0.047$	n.s.	n.s.	n.s	n.s	$P < 0.021$	n.s.

TABLE 3

Comparison with Previous Stereological Estimates of Neuronal Number in Subregions of the Male Rat Hippocampus in Control Rats Using the Optical Fractionator Technique

Hipp. Areas	Cell number	Rat strain	Age	Reference
GL	1,200,000	Wistar	30 days	West et al., 1991
	970,029	SD	221–226 days	Fitting et al., 2008
	1,172,290	SD	154–160 days	Fitting et al., present
	1,150,600	SD	Adult (300–350 g)	Grady et al., 2003[a]
	1,200,000	LE	27–28 and 6 months	Rapp and Gallagher, 1996
	1,191,580	Wistar	180 days	Sousa et al., 1997
	~944,030	Wistar	30 days	Sousa et al., 1998
	~1,182,100	Wistar	180 days	Sousa et al., 1998
DGH	530,000	Wistar	30 days	West et al., 1991
	52,425	SD	90 days	Lister et al., 2005
	51,672	SD	221–226 days	Fitting et al., 2008
	52,495	SD	154–160 days	Fitting et al., present
	65,420	SD	Adult (300–350 g)	Grady et al., 2003[a]
	46,637	Wistar	180 days	Sousa et al., 1997
	~43,803	Wistar	30 days	Sousa et al., 1998
	~45,385	Wistar	180 days	Sousa et al., 1998
CA2/3	250,000	Wistar	30 days	West et al., 1991
	181,570	SD	90 days	Lister et al., 2005
	252,504	SD	221–226 days	Fitting et al., 2008
	416,498	SD	154–160 days	Fitting et al., present
	262,200	SD	Adult (300–350 g)	Grady et al., 2003[a]
	~225,000	LE	27–28 and 6 months	Rapp and Gallagher, 1996
	241,240	Wistar	180 days	Sousa et al., 1997
	~244,647	Wistar	30 days	Sousa et al., 1998
	~239,615	Wistar	180 days	Sousa et al., 1998
CA1	380,000	Wistar	30 days	West et al., 1991
	330,998	SD	90 days	Lister et al., 2005
	233,042	SD	221–226 days	Fitting et al., 2008
	262,181	SD	154–160 days	Fitting et al., present
	387,800	SD	Adult (300–350 g)	Grady et al., 2003[a]
	~390,000	LE	27–28 and 6 months	Rapp and Gallagher, 1996
	423,950	Wistar	180 days of age	Sousa et al., 1997
	~403,930	Wistar	30 days	Sousa et al., 1998
	~420,524	Wistar	180 days	Sousa et al., 1998
Sub	198,630	SD	90 days	Lister et al., 2005
	260,148	SD	221–226 days	Fitting et al., 2008
	312,252	SD	154–160 days	Fitting et al., present

[a]Indicating the use of the optical volume fractionator; GL = granular layer; DGH = hilus of the dentate gyrus; CA3/2 = cornu ammonis fields 3/2; CA1 = cornu ammonis field 1; Sub = subiculum; SD = Sprague-Dawley rats; LE = Long-Evans hooded rats.